Bulletin of the Seismological Society of America, Vol. 92, No. 5, pp. 1737–1753, June 2002

Subsurface Geometry and Evolution of the Seattle Fault Zone and the Seattle Basin, Washington

by U. S. ten Brink, P. C. Molzer, M. A. Fisher, R. J. Blakely, R. C. Bucknam, T. Parsons, R. S. Crosson, and K. C. Creager

Abstract The Seattle fault, a large, seismically active, east–west-striking fault zone under Seattle, is the best-studied fault within the tectonically active Puget Lowland in western Washington, yet its subsurface geometry and evolution are not well constrained. We combine several analysis and modeling approaches to study the fault geometry and evolution, including depth-converted, deep-seismic-reflection images, *P*-wave-velocity field, gravity data, elastic modeling of shoreline uplift from a late Holocene earthquake, and kinematic fault restoration. We propose that the Seattle thrust or reverse fault is accompanied by a shallow, antithetic reverse fault that emerges south of the main fault. The wedge enclosed by the two faults is subject to an enhanced uplift, as indicated by the boxcar shape of the shoreline uplift from the last major earthquake on the fault zone. The Seattle Basin is interpreted as a flexural basin at the footwall of the Seattle fault zone. Basin stratigraphy and the regional tectonic history lead us to suggest that the Seattle fault zone initiated as a reverse fault during the middle Miocene, concurrently with changes in the regional stress field, to absorb some of the north–south shortening of the Cascadia forearc. Kingston Arch, 30 km north of the Seattle fault zone, is interpreted as a more recent disruption arising within the basin, probably due to the development of a blind reverse fault.

Introduction

The M_w 6.9 1995 Kobe, Japan, earthquake and the resulting devastation have focused attention on the seismic hazard from crustal faults in forearc regions of subduction zones. In the United States, there has been a growing realization of seismic hazard from crustal faults in the Puget Lowland, a densely populated, forearc region of the Cascadia subduction zone in western Washington State. However, the extent of crustal deformation and seismic hazard in the Puget Lowland are not well understood, partly because the underlying tectonic forces are not fully understood and partly because of the extensive cover of glacial deposits and forests.

Many workers believe that the Seattle fault zone, an east–west-oriented reverse fault passing under Seattle (Fig. 1b), is one of the faults accommodating the north–south shortening of the Cascadia forearc. Geologic and paleomagnetic data indicate clockwise rotation of the Cascadia forearc since the middle Miocene (Wells *et al.*, 1998), and geodetic data indicate a northward migration of the forearc at a rate of several millimeters per year, relative to stable North America (Khazaradze *et al.*, 1999). The forearc motion has been linked to the northward translation of the Sierra Nevada block in California as a result of Basin-and-Range extension and Pacific–North America dextral shear (Pezzopane and Weldon, 1993; Walcott, 1993; Fig. 1a). The northward migration of the Cascadia forearc is probably accommodated by crustal shortening against the backstop of the Canadian Coast Ranges and, according to some, by the uplift of the Olympic Mountains (Walcott, 1993; Wells *et al.*, 1998).

The shortening in the Puget Lowland is expressed as upper crustal deformation into a series of 30–50-km-wide structural highs and basins, of which the Seattle Basin is the deepest (Johnson *et al.*, 1996; Pratt *et al.*, 1997; Brocher *et al.*, 2001). Pratt *et al.* (1997) proposed the existence of a detachment surface at 14–20-km depth under the Puget Lowland along which the shortening is accommodated. The Seattle Basin and Kingston Arch were interpreted to be the shallow manifestations of a ramp in this detachment, and the Seattle fault zone was interpreted as a fault branching from the detachment (Pratt *et al.*, 1997). Brocher *et al.* (2001) suggested that shortening takes place along steeply dipping reverse faults with opposing dips that bound these highs and lows. The faults penetrate to depths of 25–30 km, are not interconnected, and are perhaps reactivated normal faults (Brocher *et al.*, 2001).

Seismic activity under the Puget Lowland can also be attributed to the north–south shortening of the forearc. It is perhaps concentrated within the Puget Lowland because

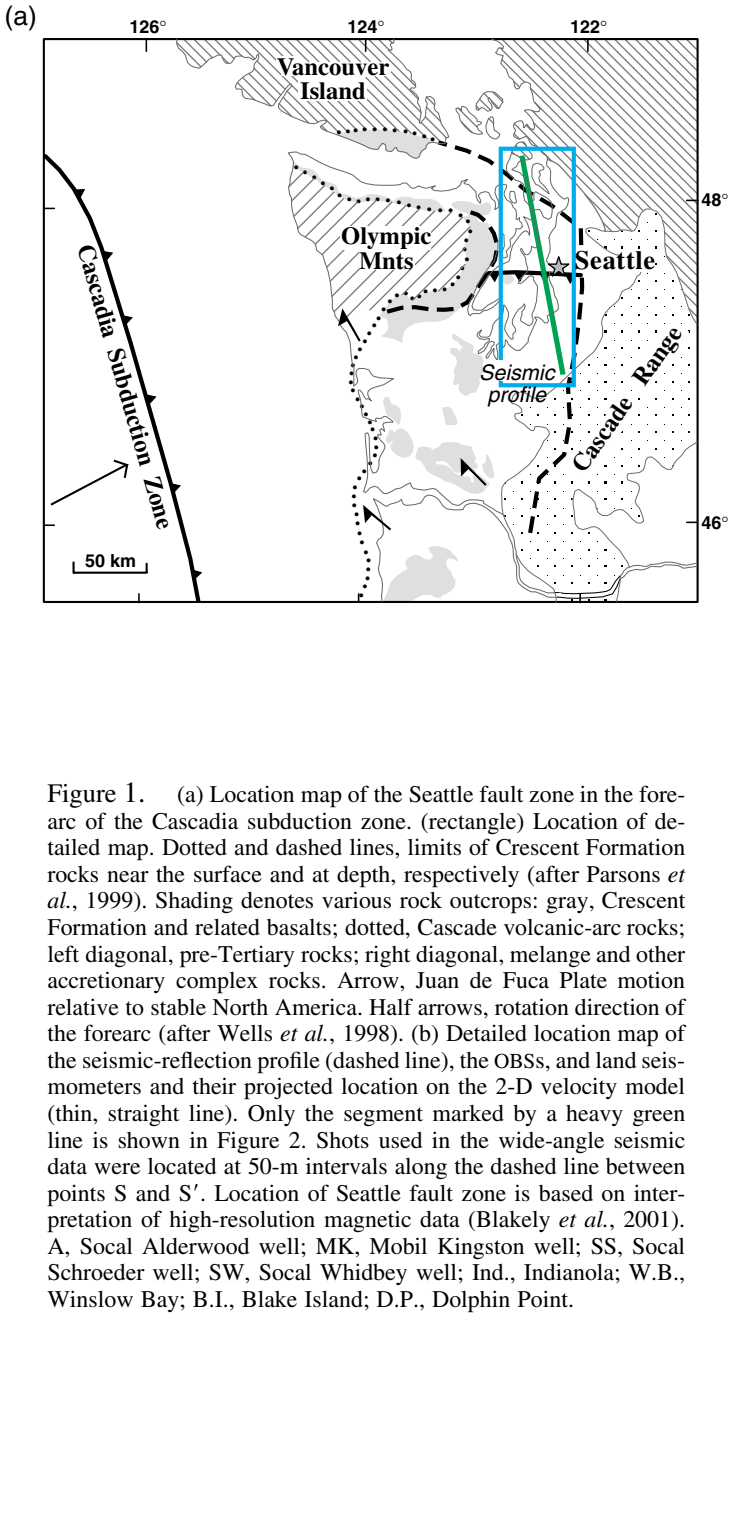

Figure 1. (a) Location map of the Seattle fault zone in the forearc of the Cascadia subduction zone. (rectangle) Location of detailed map. Dotted and dashed lines, limits of Crescent Formation rocks near the surface and at depth, respectively (after Parsons *et al.*, 1999). Shading denotes various rock outcrops: gray, Crescent Formation and related basalts; dotted, Cascade volcanic-arc rocks; left diagonal, pre-Tertiary rocks; right diagonal, melange and other accretionary complex rocks. Arrow, Juan de Fuca Plate motion relative to stable North America. Half arrows, rotation direction of the forearc (after Wells *et al.*, 1998). (b) Detailed location map of the seismic-reflection profile (dashed line), the OBSs, and land seismometers and their projected location on the 2-D velocity model (thin, straight line). Only the segment marked by a heavy green line is shown in Figure 2. Shots used in the wide-angle seismic data were located at 50-m intervals along the dashed line between points S and S′. Location of Seattle fault zone is based on interpretation of high-resolution magnetic data (Blakely *et al.*, 2001). A, Socal Alderwood well; MK, Mobil Kingston well; SS, Socal Schroeder well; SW, Socal Whidbey well; Ind., Indianola; W.B., Winslow Bay; B.I., Blake Island; D.P., Dolphin Point.

basement there is made of the rigid, mafic Siletz terrane, which undergoes brittle deformation, whereas the forearc to the west (the Olympic Peninsula) is made of the more ductile, accretionary complex, which deforms aseismically (Crosson *et al.*, 1999). An alternative seismotectonic framework for the forearc in western Washington suggests, however, that the uplift of the Olympic Mountains is due to the underlying upwarp in the subducted Juan de Fuca Plate, coupled with an unusually high flux of accreted sediments into the trench at this location (Brandon *et al.*, 1998). The semi-

circular arrangement of basins in the Puget Lowland around the eastern Olympic Mountains and their tilt away from the mountains may point to a genetic relationship between the basins and mountain uplift (Crosson and Symons, 2001).

A wealth of new information about the subsurface geology of the Puget Lowland helps define the deformation and seismic hazard of this region. The information includes released proprietary data (Johnson *et al.*, 1994; Pratt *et al.*, 1997; Brocher and Reubel, 1998; Johnson *et al.*, 1999; Rau and Johnson, 1999) and new data, much of it collected during the various phases of the Seismic Hazards Investigation of Puget Sound (SHIPS) experiment (Brocher *et al.*, 2001, and references therein). Despite these efforts, considerable uncertainty remains about the geometry and evolution of the faults cutting the Puget Lowland. Microseismicity is sparse and, to date, does not reveal planar faults [Brocher *et al.*, 2001; van Wagoner *et al.*, 2002]. The spatial resolution of 3D seismic tomographic studies (Brocher *et al.*, 2001; van Wagoner *et al.*, submitted) is insufficient to define the subsurface geometry of faults. Existing seismic-reflection data typically penetrate only to shallow depths (Johnson *et al.*, 1999), and deeper reflection lines lack velocity control (Johnson *et al.*, 1994; Pratt *et al.*, 1997). For these reasons, even the subsurface geometry of the Seattle fault zone, the best-studied crustal fault in the Puget Lowland, is still debated.

The 4–7-km-wide and 60–65-km-long Seattle fault zone is outlined across the Puget Lowland by a set of magnetic anomalies over the hanging wall of the fault (Blakely *et al.*, 2001), by a steep gravity slope (Finn, 1990; Pratt *et al.*, 1997), and by lateral velocity contrast (Brocher *et al.*, 2001; van Wagoner *et al.*, submitted). The fault zone separates the thick, sedimentary sequence of the Seattle Basin to the north from the thin, sedimentary cover and shallow basement rocks south of the fault, indicating a long history of fault activity. Paleoseismic evidence indicates Holocene displacement on the fault, including an estimated magnitude 7 earthquake at 900–930 A.D. (Yount and Gower, 1991; Atwater and Moore, 1992; Bucknam *et al.*, 1992).

Various dips were proposed for the Seattle fault zone. Johnson *et al.* (1994, 1999) proposed a mean dip of 45°–60° for the top 6 km of the fault and 45°–65° for the top 1 km based on industry and high-resolution seismic-reflection data, respectively. Calvert and Fisher (2001) proposed a dip of 60° for the top 1 km of the fault based on *P*-wave velocities from seismic-reflection data. Using different industry data, Pratt *et al.* (1997) proposed a dip of 45° for the top 6 km, shallowing to 20°–25° at depths of 6–16 km. Both Johnson *et al.* (1994, 1999) and Calvert and Fisher identified four subparallel, south-dipping fault strands in the Seattle fault zone. Although the northernmost strand is presumed the most active since the Quaternary, other strands are still active, with either reverse or normal slip (Johnson *et al.*, 1994). Brocher *et al.* (2001) favored an unspecified steep dip (>65° in their figures) extending to a depth of 28 km. Projected epicenters from the earthquake catalog delineate a diffuse zone of seismicity with an even higher dip, 70°–80°, extending from the surface location of the Seattle fault zone to a depth of 25 km (Fig 2b; van Wagoner *et al.*, submitted). Based on focal mechanisms of small earthquakes along the Seattle fault zone, van Wagoner *et al.* (submitted) proposed that the Seattle fault zone is south-dipping with a subvertical dip and that the fault has recently been reactivated as a normal fault (i.e., north side up).

It is apparent from the preceding discussion that opinions diverge regarding the Seattle fault geometry, the style of upper crustal deformation, and the driving force for motion on the fault, and these impact the ability to assess the seismic hazard of the Seattle fault. Here we present results from a combination of independent observations and modeling methods, some of which have not been previously applied to the study of the Seattle fault. We model seismic-refraction data collected during the 1998 offshore–onshore SHIPS experiment for a detailed *P*-wave-velocity structure. We interpret the velocity contours to delineate the fault zone and the depth of the Seattle Basin and the velocity field to convert coincident deep-penetrating reflection data to depth and to model a coincident gravity profile. Using an elastic dislocation model, we explore the permissible range of fault geometries that could generate the observed shoreline uplift from a large earthquake ~1,100 years ago. Kinematic fault models that produce the observed structure and honor the surface geology are then used to explain the fault-zone evolution in relation to the north–south shortening of the Puget Lowland. The stratal geometry of the basin is used to argue for a younger age for fault initiation than previously suggested. It is important to note that we are presenting a 2D cross section along the Puget Sound for structures that vary in their relief along strike (e.g., Blakely *et al.*, 2001; Brocher *et al.*, 2001).

Tectonic Framework and Geologic Background

The Puget Lowland is located in the interior part of the forearc region of the Cascadia subduction zone (Fig. 1a) between the Cascade volcanic arc and older Mesozoic terranes to the east and the north and the uplifted and exhumed accretionary complex of the Olympic Mountains to the west. The Puget Lowland is underlain to a depth of 25–30 km by the Siletz terrane (Symons and Crosson, 1997), basalts and intrusive rocks with island-arc composition that were accreted to North America 50–62 m.y. ago (Duncan, 1982). The Siletz terrane increases in width and thickness in southern Washington and in Oregon (Trehu *et al.*, 1994; Parsons *et al.*, 1999). Tilted exposures of the Siletz terrane wrap around the Olympic accretionary complex (Brandon *et al.*, 1998) and appear to be underthrust by the accretionary complex (Symons and Crosson, 1997).

Basement rocks under the Seattle Basin were drilled at Mobil Kingston well (see Fig. 1b for location) at a depth interval of 2,195–2,637 m (Fig. 2b; Rau and Johnson, 1999) and consist of basalt interbedded with siltstone, tuff, and

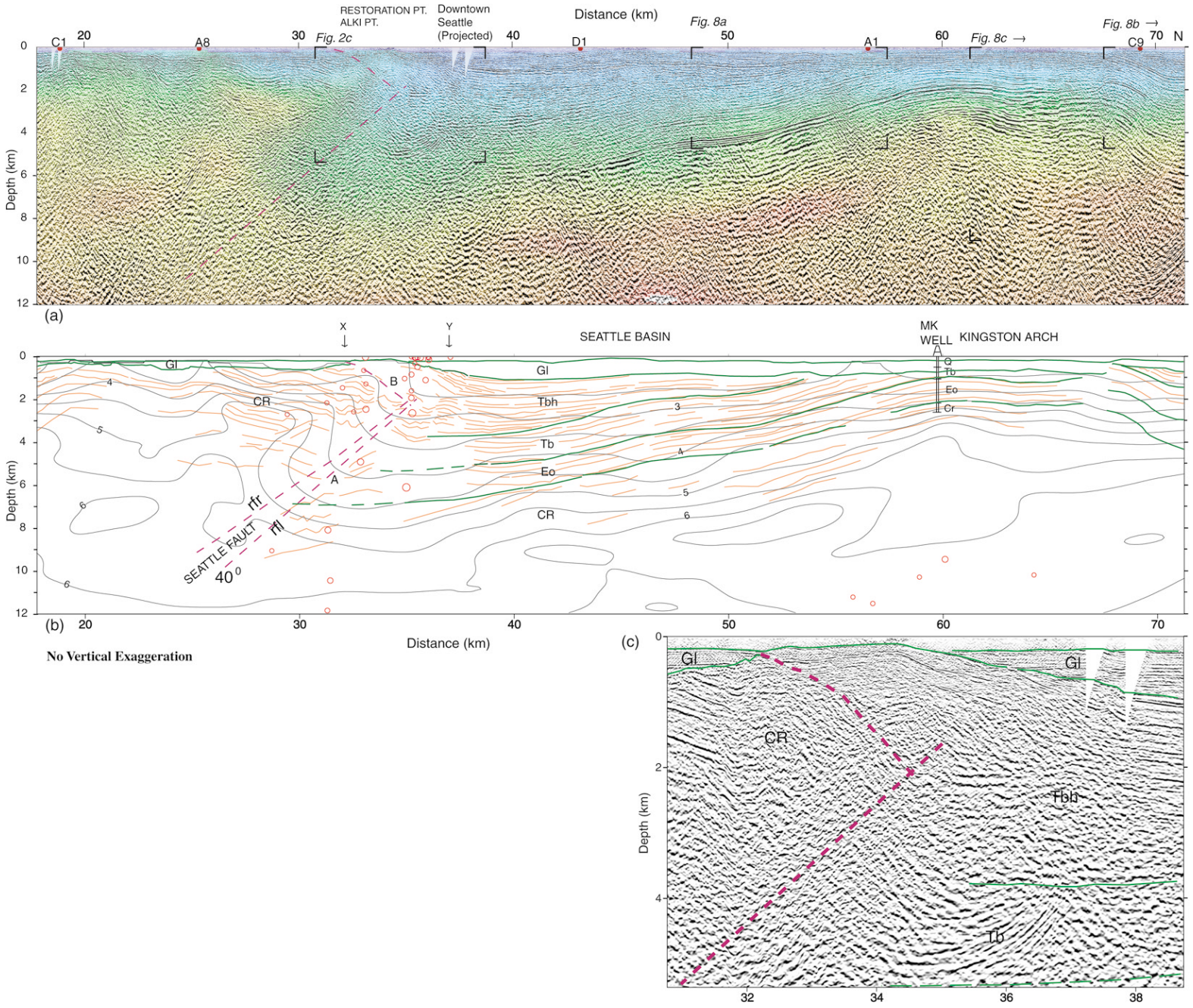

Figure 2. (*Caption on facing page.*)

Figure 2. (a) A section of seismic-reflection line (black and white) and coincident *P*-wave-velocity model (color) along Puget Sound. See Figure 1b for location. (b) Line-drawing interpretation of the seismic reflections (thin, red lines) and isovelocity contours at 0.5-km/sec intervals (thin, black lines) of the section shown in (a). Also shown are projected locations of earthquakes within 0.1° of the velocity model (red circles), chronostratigraphic boundaries (heavy, green lines), and interpreted faults (dashed red lines) from seismic-reflection (marked rfl) and from seismic refraction (marked rfr) data. Simplified stratigraphy of Mobil Kingston well (Rau and Johnson, 1999) is projected onto the seismic reflection profile to aid with stratigraphic interpretation. Formation abbreviations are Cr, Crescent; Eo, Eocene undifferentiated sediments; Tb, Blakeley; and Tbh, Blakely Harbor. Movement along fault strands marked A and B is discussed in Figure 6. Location of points *x* and *y* is marked in Figure 1b. (c) Enlargement of the seismic-reflection profile with interpretation. Location of enlargement marked by a frame in (a).

conglomerate. In a second drill hole (Socal–Whidbey), mafic rocks were found to interfinger with sandstone (Rau and Johnson, 1999). The mafic rocks form part of the Siletz terrane, known locally as the Crescent Formation.

Based on ties to the Mobil Kingston well, the lowermost 1–1.5 km of sediments in the Seattle Basin are probably Eocene marine strata deposited in upper to middle bathyal depths (Johnson *et al.*, 1994). However, adjacent wells show large variations in depositional environment and thickness (Rau and Johnson, 1999), owing either to the location of the region close to a narrow continental shelf in the forearc or to tectonic movements. The Eocene interval is overlain by turbidites of the Upper Eocene–Oligocene Blakeley Formation, which were deposited at bathyal depths (Johnson *et al.*, 1999). The Blakeley Formation is exposed and tilted at near-vertical dips along the Seattle fault, where it attains a thickness of 2,130 m (Fulmer, 1975). Only a 500-m-thick section belonging to the lower member of the Blakeley Formation is encountered at the Mobil Kingston well on the Kingston Arch, and stratal geometry indicates that the upper part of the formation was eroded prior to Quaternary deposition (Johnson *et al.*, 1994). The nonmarine Miocene Blakeley Harbor Formation, perhaps 1,040 m thick in total, overlies the Blakeley Formation rocks in southeastern Bainbridge Island (Fulmer, 1975). It is missing from nearby deep wells (Rau & Johnson, 1999). Quaternary sediments, mostly glacial, cover most of the lowland.

Seismic Data

We analyze a subset of the data from the 1998 SHIPS experiment collected along the Puget Sound (Fig. 1). These data include a 90-km-long seismic-reflection profile shot at 50-m intervals by the R/V Thompson using a 79.3-liter (4838 cu. in.) air-gun array and recorded by a 2.4-km-long, 96-channel digital seismic streamer. The reflection profile was processed routinely and migrated after stack using Kirchhof migration. The same shots were also recorded by six U.S. Geological Survey ocean-bottom seismometers (OBSs) and 13 land seismometers (Fig. 3), producing a coincident 145-km-long, wide-angle seismic-reflection–refraction profile (Fig. 1b). We selected those shots located between points S and S′ in Figure 1b and projected them onto the central 70-km-long segment of the profile. The quality of the records is generally high, as seen in Figure 3. There was a significant reduction in the energy transmitted across the Seattle fault zone in some of the stations (UW50, C1, C9, A1017, and A1011), which we attribute to diffractions from the fault zone. First arrivals from all shots fired between points S and S′ were identified in all but eight stations (Fig. 4). A significant (1.5-sec) offset in the first arrival is observed across the Seattle fault zone (Fig. 3) and is attributed to the contrast between sedimentary rocks north of the fault zone and the mafic rocks south of the fault zone.

The velocity model was derived as follows. The starting velocity model, 90 km long and 25 km thick, was derived from forward raytracing of arrivals for the 6 OBSs using Zelt's raytracing code (Zelt and Smith, 1992) with the RayGUI interactive interface (Loss *et al.*, 1998). The resultant model was gridded at 100 m, smoothed using three iterations of a 2D median filter with a 20 × 20 cell window, and extrapolated north and south to a new velocity model, 145 km long. The new velocity grid consisting of 1,450 × 252 grid cells, was used as the input velocity model for a first-arrival tomographic inversion from all six OBSs and 13 land seismographs. The tomography used a graph method for forward modeling and a conjugate-gradient approach for model update (Zhang and Toksoz, 1998). The model roughness as part of the objective function was allowed to increase during subsequent iterations.

The wide-angle data were modeled to produce a *P*-wave-velocity structure that fits the travel times of all data, with a root-mean-square misfit of 120 msec (Fig. 4). The misfit applies to the entire 145-km-long model, half of which is located onshore, where we have neither ray reciprocity nor constraints from seismic-reflection data. Therefore, we focus our discussion and presentation (Figs. 2, 5, and 6) on the coincident seismic-reflection and refraction portion of the model, which is well constrained by dense, reciprocating ray coverage and by the reflection image. Though not formally calculated, the misfit in this part of the model is lower. The absence of a recording station directly above the fault zone affects only the reciprocity of rays traveling through the shallowest 1–2 km of the fault zone, whereas the deeper parts of the fault zone are well covered by stations D1 and A8 and by more distal stations.

The velocity structure was used to convert the reflection profile from time to depth. The velocity structure, plotted in color, was superposed on the depth-converted multichannel seismic reflection (MCS) profile, plotted in black and white

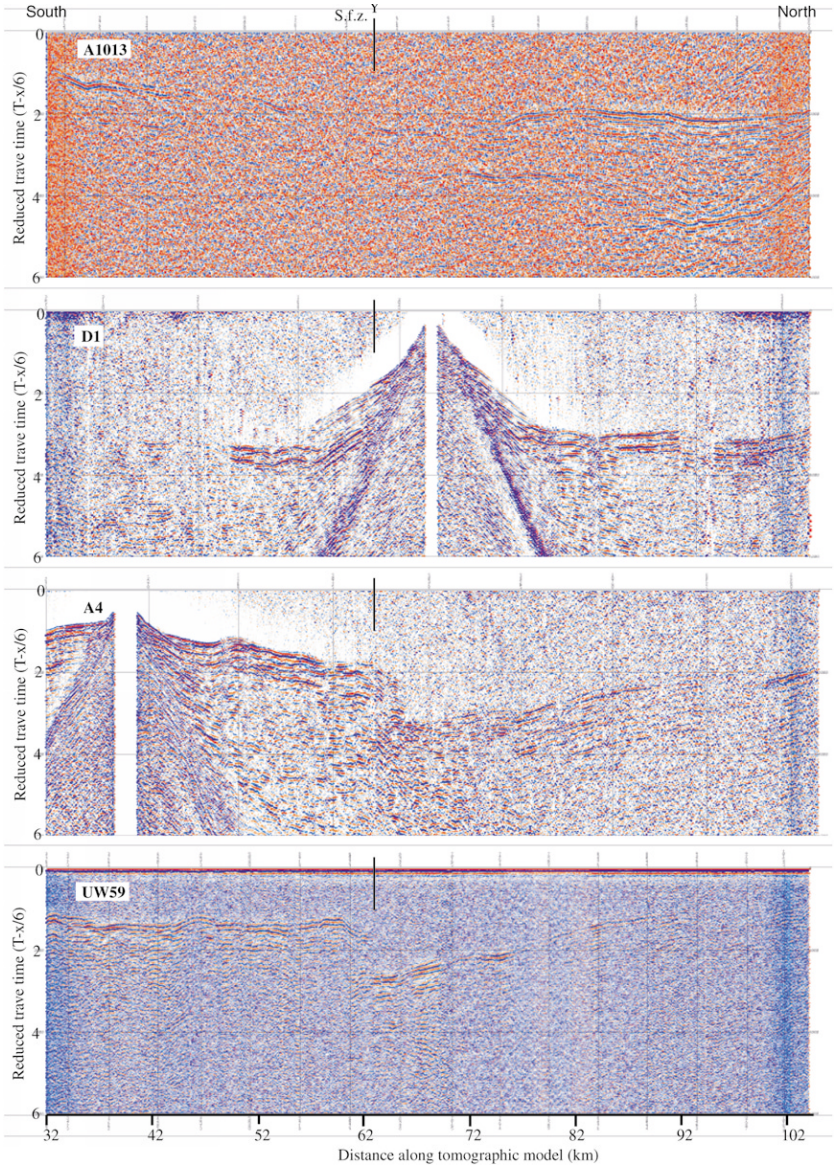

Figure 3. Common-receiver gathers for selected OBSs and land seismometers. Seismic sources are airgun shots at 50-m spacing located along the seismic-reflection profile between points S and S′ (see Fig. 1b for location). Data are plotted with a reduced travel time, $Tr = T - X/V$, where T is the original travel time, X is shot–receiver offset in km, and, V, the velocity, = 6 km/sec. See Figure 1 for location of OBSs and of point *Y*. Time delay in the first arrival in the vicinity of the Seattle fault zone (S.f.z.) is due to lateral velocity contrasts between the basin fill in the footwall and Crescent Formation basalt in the hanging wall. Distance scale represents the projection of both shots and receivers onto a single line, and therefore, the seismic records cannot be aligned perfectly.

(Fig. 2). This procedure facilitates the interpretation of both reflection geometry and velocity anomalies at their true depth. Care was exercised to properly project the velocity model onto the MCS profile where they diverge in space (Fig. 1b). The traces of the velocity model and the MCS profile across the Seattle fault are identical. The velocity grid was also converted to a density grid, and a gravity profile was calculated and compared with the observed data (Fig. 5).

The Seattle Basin

Simulations of ground motion for hypothetical earthquakes along the Seattle fault highlight the importance of the basin's geometry in modulating long-period ground motion (Frankel and Stephenson, 2000). The combined seismic-reflection, seismic-refraction, and gravity methods provide an accurate estimate of the geometry of the Seattle Basin along Puget Sound. Previous determinations relied either on seismic-reflection data with a single, assumed velocity profile (Johnson *et al.*, 1994; Pratt *et al.*, 1997) or on lower-resolution, 3D seismic tomography (Brocher *et al.*, 2001). On our seismic-reflection profile, basement can be clearly identified only in some parts (e.g., around km 50, Fig. 2a). This is because the top of the Crescent Formation consists of interbedded volcanic and sedimentary rocks, which tend to generate horizontally continuous reflections. The *P*-wave-velocity field superposed on the seismic-reflection data provides a better guide to basement identification.

Basement is defined within the velocity range of 4.0–4.5 km/sec, and basin depth increases from the Kingston Arch, where it is <2.5 km thick, to ~7 km under the front of the Seattle fault zone (Figs. 2 and 5). The low end of the

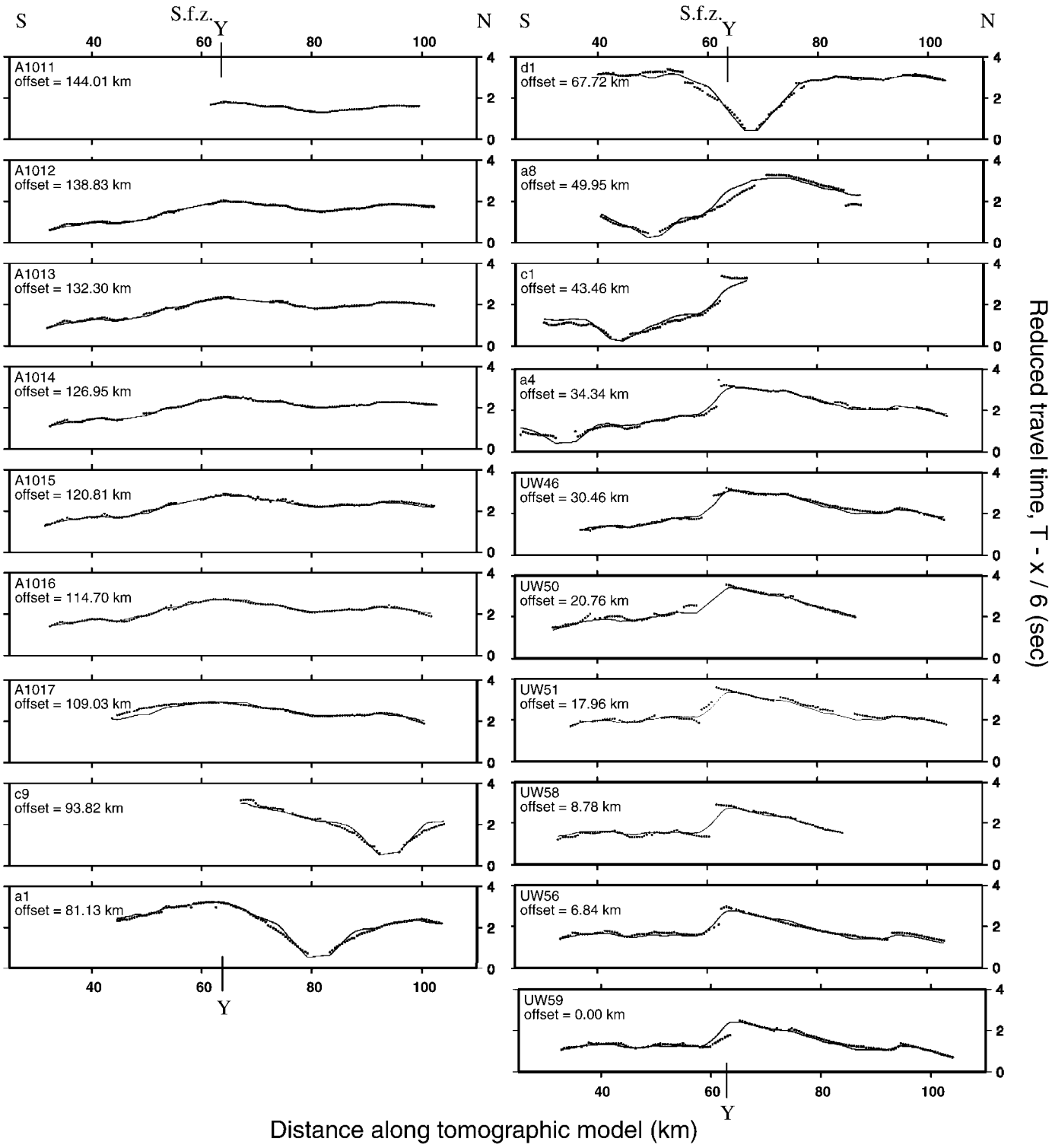

Figure 4. Observed travel times (dots) and calculated travel time (lines) from the first-arrival tomographic inversion model for every receiver plotted. Secondary arrivals were not modeled. Reduced travel time is similar to Figure 3, but time axis increases upward. See Figure 1 for location of OBSs, land stations, and point *Y*. S.f.z., Seattle fault zone. Distance scale represents the projection of both shots and receivers onto a single line (thin, straight line in Fig. 1b), and therefore, the seismic records cannot be aligned perfectly.

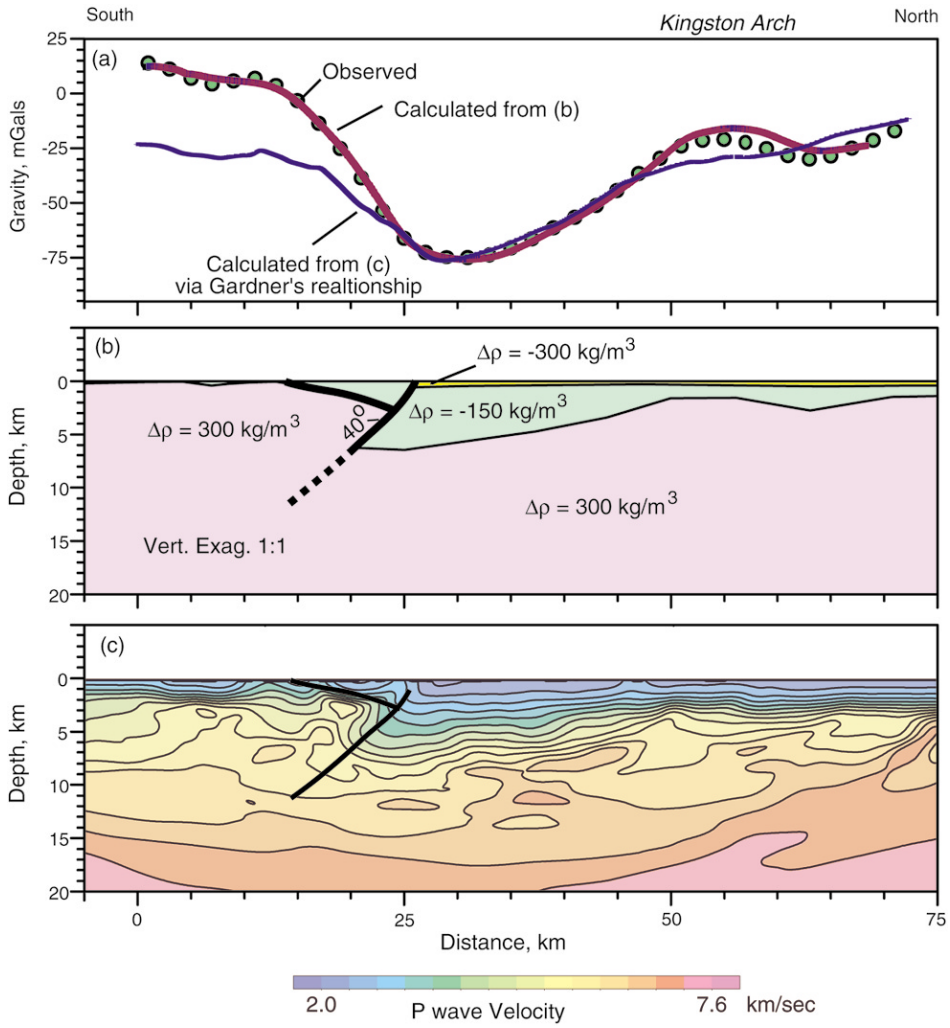

Figure 5. (a) Observed and calculated Bouguer gravity anomaly for different density models (b, c) along the seismic profile, emphasizing the need for high-density Crescent Formation rocks to occupy almost the entire hanging wall of the Seattle fault zone. (b) A density model with Crescent Formation rocks occupying the hanging wall of the Seattle fault zone. (c) Tomoraphic velocity model (similar to Fig. 2) used to calculate a density grid according to the relationship density = 1,741 × velocity$^{0.25}$ (Gardner *et al.*, 1974). Calculated gravity anomaly from this grid is shown by blue line in (a).

velocity range (4.0 km/sec) is associated with basement at shallow depths under the Kingston Arch, and the high end (4.5 km/sec) with basement at the deep end of the basin where compaction is expected to be the largest. By extrapolation from surrounding drill holes (Rau and Johnson, 1999), the lowermost fill of the Seattle Basin comprises Eocene sandstones and siltstones. Their velocity in sonic logs from drill holes in Puget Sound is <4.5 km/sec (Brocher and Ruebel, 1998). Sandstone, in general, rarely reaches velocities >4.5 km/sec, even under 7 km of overburden, and other clastic rocks always have much lower velocities (e.g., Gueguen and Palciauskas, 1994, pp. 159–168). Of particular interest is whether the Eocene sequence thickens toward the Seattle fault. We place the basement at km 30–35 along the 4.5-km/sec velocity contour because of the clastic composition of the lowermost sediments. Velocities in this region of the model are well resolved by reciprocating diving waves to stations north and south of the fault.

Our stratigraphic interpretation of the Seattle Basin follows those of Johnson *et al.* (1994) and Pratt *et al.* (1997). Their interpretations of the Eocene and Blakeley Formation interval were tied to the Mobil Kingston #1 borehole on Kingston Arch, and the identification of a wedge of Blakely Harbor Formation within the basin was inferred from outcrops of Blakely Harbor rocks along the southern and southeastern parts of Bainbridge Island.

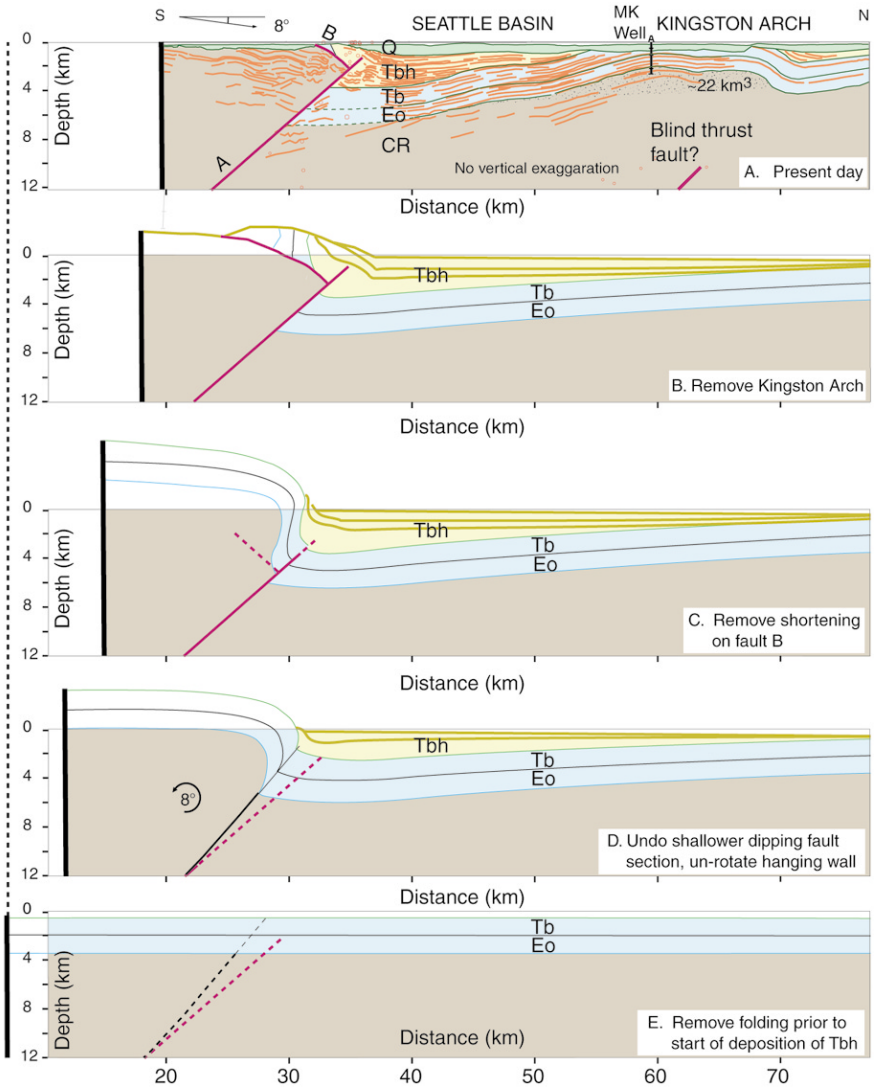

Figure 6. Step-by-step geometric restoration of the Seattle fault zone, Seattle Basin, and Kingston Arch to their preshortened positions. Thin and thick black lines, fold axis or an earlier, steeper fault than fault A. See text for detailed explanation. Uplift of Kingston Arch is dotted in (a). Other symbols as in Figure 2b.

Subsurface Geometry of the Seattle Fault Zone from Seismic and Gravity Data

The seismic-reflection profile (Fig. 2c) shows a 2-km-wide zone of chaotic reflections with a few reflectors dipping to the south. Our seismic-reflection profile as well as previous profiles (Johnson *et al.*, 1994; Pratt *et al.*, 1997) failed to image clear fault-plane reflections. The lack of well-identified fault-plane reflections is not unusual, because the existence of reflections depends on the width and length scale of heterogeneities in relation to the acoustic frequency. The dashed line marked A in Figure 2b defines a possible location and dip (~40°) of the Seattle fault zone. It passes between continuous basement reflections to the south of the fault and reflections in the Seattle Basin to the north of the fault (Fig. 2). A dipping reflection with shallower dip (25°–30°) is observed at a depth of 3–4 km around km 30, but its relationship to the fault zone is not clear. Near-surface seismicity and truncated and tilted reflections (Fig. 2c) probably mark the upper end of the fault.

We can also define the location and dip of the fault zone by using the *P*-wave-velocity contours by connecting the concave-upward inflections in the velocity contours (dotted line in Fig. 2b) under the assumption that the hanging wall of the fault mainly comprises Crescent Formation basalt and the footwall contains Seattle Basin sedimentary rocks. The fault dip defined by the velocity model under this assumption is ~35°–40°.

The gravity data (Fig. 5) suggest that the hanging wall of the Seattle fault zone contains higher-density rocks (crescent formation) than the footwalls (clastic sediments). This

higher density is only because of higher velocities in the hanging wall than in the footwall, as indicated by the refraction data (Fig. 5c). It also reflects different rock composition across the fault. The calculated anomaly (thin line in Fig. 5a) underestimates the observed anomaly in the hanging wall by as much as 40 mGal; we simply convert velocity to density, using a velocity–density ratio for sediments (density = 1,741 × velocity$^{0.25}$) (Gardner *et al.*, 1974). Laboratory measurements of Crescent Formation basalt (Brocher and Reubel, 1998) confirm that the proportionality factor between density and velocity in these rocks is higher than for sediments; density = ~1,840 × velocity$^{0.25}$. We therefore use basement density south of the Seattle Fault (Fig. 5b). According to the gravity model, the fault dip between depths of 2.5 and 7 km is ~40°.

Antithetic Fault and the Dislocation Model

We propose that an antithetic fault strand (a backthrust) emerges north of Blake Island and connects at a depth of 2.5–3.5 km with the main fault trace (fault B, Fig. 2). Shoreline uplift along the Puget Sound from a large earthquake on the Seattle fault zone (Bucknam *et al.*, 1992) at ~900–930 A.D. provides an independent evaluation of the geometry of the Seattle fault zone and, in particular, the existence of a backthrust. This earthquake produced a prominent, raised shoreline and marine terrace that fringe much of the coast over the hanging wall of the fault. We use the shoreline as a horizontal datum that defines the pattern of vertical deformation produced by the earthquake. Due to the limited distribution of shorelines in the vicinity of the Seattle fault zone, the uplift pattern can be documented only along a 20-km-wide portion of the Seattle fault zone, where it appears to be relatively uniform in an east–west direction [Bucknam *et al.*, 1999].

We model the uplift along a north–south profile located at the western shore of Puget Sound (longitude 122°30′, Fig. 1b), assuming for simplicity that all of the uplift is coseismic and neglecting a rise in sea level (~1 m; Sherrod *et al.*, 1999). This profile contains most of the measurements in the area (ten Brink and Bucknam, unpublished data) and is roughly centered at the fault. The observed uplift has a distinct boxcar shape of a narrow, high-amplitude uplift, which abruptly decreases to about one-sixth of its value over 3 km to the south and continues to decrease gradually southward (Fig. 8). To the north, the uplift changes abruptly to subsidence.

We model the uplift by using a dislocation model in elastic half-space (Toda *et al.*, 1998), assuming that our profile is located at the center of a 65-km-long fault. The distinctively narrow zone (7 km) of almost-constant-amplitude uplift (6–7 m) cannot be fit with a single thrust fault, regardless of dip (Fig. 9). A single thrust fault is predicted to generate a sawtooth shape, that is, a gradually decreasing uplift south of the maximum uplift, which should be located close to the surface projection of the fault (e.g., King *et al.*, 1988). The observed shoreline uplift, on the other hand, reaches its maximum at km 4.5, close to the south end of the narrow uplift, before dropping abruptly to the south. (Km 0 in Figure 8 corresponds to the intersection of longitude 122°30′ with the red dashed line in Fig. 1b.) We can fit this distinctive shape with simultaneous motion along a thrust fault and an antithetic reverse fault, which together lift the enclosed wedge almost vertically. The upper tip of the modeled backthrust ~6.5 km south of the upper tip of the Seattle fault zone is constrained by the location of the abrupt drop-off at the south end of the narrow, high-amplitude uplift. The 40° ± 10° dip of the backthrust is constrained by the slope of the uplift as defined by the two points south of the drop-off (marked BI and DP in Figs. 1 and 8). A more detailed analysis of the uncertainties in dip determination and an estimate of the slip on the two fault strands are given elsewhere (ten Brink and Bucknam, unpublished data.).

The wavelength of the subsidence north of the fault trace is indicative of the fault dip (regardless of the existence of a backthrust). The absence of subsidence at Indianola (B. Sherrod, personal comm., 2000; see Fig. 1 for location) and the small amplitude of subsidence at Winslow Bay immediately north of the surface trace of the Seattle fault zone constrain the dip of the fault to 35°–50° (Fig. 8). Models with low dips (e.g., 20°, Fig. 9) predict very little subsidence of the footwall in contrast to the observations. Models with high fault dip (e.g., 60° and 70°, Fig. 9) fit the subsidence at Winslow Bay and at West Point only if we assume that Winslow Bay is an intermediate point between maximum subsidence at West Point and uplift south of Winslow Bay. However, such models require the surface trace of the Seattle fault zone to be located between Winslow Bay and West Point, which is not supported by seismic-reflection data and geologic observations. The surface trace of the Seattle fault zone is located south of Winslow Bay on both sides of Puget Sound (Johnson *et al.*, 1999). Additionally, models with a high fault dip predict subsidence at Indianola, which is not observed (Fig. 9). Models with moderate dips of 35°–50° do not fit the subsidence at West Point, which is larger than that at Winslow Bay (Fig. 8). Because West Point is farthest offline of all the projected measurements along our 2D model (Fig. 1), we chose to fit two points (Indianola and Winslow Bay) and the known location of the surface trace of the fault south of Winslow Bay and ignore West Point.

Lateral change in the characteristic reflectivity of the backthrust in the seismic-reflection data (Fig. 2c) may be due to rotation and internal deformation within the wedge. A weak, north-dipping reflector coincident with fault B is also observed in the seismic-reflection data. The gravity model (Fig. 5) also indicates the presence of lower-density rocks in the wedge between the main fault and the antithetic fault. However, the dip of the antithetic fault in the gravity model is lower than inferred from Figures 2 and 8, probably because of deviations from a 2D geometry in the shallow

distribution of water, glacial sediments, and preglacial sediments around the fault zone (Blakely *et al.*, 2001). Slight variations in the geometry of the antithetic fault between Figures 2 and 8 are probably due to the fact that Figure 2 is a profile within Puget Sound, whereas Figure 8 is projected along the western shore of the Sound.

Evaluation of Previous Interpretations

Johnson *et al.*, (1994, 1999) and Calvert and Fisher (2001) interpreted seismic-reflection data across the Seattle fault zone as showing three or four subparallel, south-dipping fault strands (Fig. 9a, 9c). A synthetic (subparallel) geometry implies the presence of trapped, stacked, tilted sedimentary sections with considerable thickness (8 km) between the fault strands at the hanging wall of the present fault (Fig. 9a). The observed high densities and high velocities at the hanging wall below a depth of 2.5 km argue against this prediction.

We also tested the multiple-strand geometry against the shoreline-uplift data by using the dislocation model discussed previously. In Figure 9, we model the geometry proposed by Calvert and Fisher (2001) of three parallel faults spaced ~1 km apart and dipping 60° to the south. We divide the slip equally among the three faults. The modeled uplift shape, a sawtooth, is similar to that obtained from a single fault and is unlike the shape of the shoreline uplift. The fit cannot be improved by changing the dip, by assuming that most of the motion occurred on one of the faults, or by increasing the spacing of the faults. As the spacing among the faults is increased, the predicted uplift shape becomes a superposition of several sawteeth, with a local maximum above each fault and a gradual decay southward.

Our interpretation of the seismic-reflection and refraction data and the shoreline-uplift data from the Holocene earthquake are incompatible with the observed steeply dipping, diffuse zone of microseismicity in the vicinity of the Seattle fault zone (Brocher *et al.*, 2001) and with the suggestion that they indicate normal motion along the fault (van Wagoner *et al.*, submitted). The locations of the microseisms do not define a clear fault plane and are located within the sedimentary sequence of the Seattle Basin (Fig. 2). Our explanations for this discrepancy are that either the microseismicity is occurring on an unknown structure or that microseismicity does not provide information about the Seattle fault zone. A situation similar to the latter exists along the San Francisco Peninsula section of the San Andreas Fault, where microseismicity is located in a zone several kilometers wide on either side of the fault but is absent under the fault trace (Zoback *et al.*, 1999).

Kingston Arch Activity

The Kingston Arch is a structural high disrupting the Seattle Basin ~30 km north of the Seattle fault zone. Quaternary motion along the arch has been suggested on the basis of relatively shallow basement and microseismicity (Gower *et al.*, 1985; Pratt *et al.*, 1997). The stratal geometry of the Seattle Basin supports this suggestion. Coseismic loading by reverse motion on a rigid plate should create a basin with a diagnostic flexural shape at the footwall of a fault (e.g., King *et al.*, 1988). Blakely Harbor deposits thicken toward the fault and are tilted southward, indicating deposition during flexural deformation. (See also the section on fault age in this report.) However, the beds farthest from the Seattle fault zone (km 49–52; Fig. 7a) are much steeper than expected in a flexural basin. The tilt of the basin fill is subparallel to the tilt of the prebasin Eocene–Oligocene strata on both sides of the arch (km 49–52 and 68–70, Fig. 7a,b), indicating that tilting occurred after the deposition of Blakely Harbor sediments. In fact, the Quaternary glacial layer, which truncates the basin fill, appears to be offset near km 69. We therefore propose that localized uplift of the Kingston Arch during the Quaternary has modified the flexural deformation of the basin. A better constraint on the age of activity requires drilling into the tilted strata.

Kinematic Fault Model

Figure 6 shows a geometric restoration of the Seattle fault zone, Seattle Basin, and Kingston Arch. This kinematic model provides an alternative scenario to that of Johnson *et al.* (1994, 1999) and Pratt *et al.* (1997) and is consistent with the geophysical observations, the surface geology, and current theories of fault-propagating folds (Erslev, 1991; Allmendinger, 1998). Because the hanging wall is eroded into Crescent Formation basement, it is impossible to quantitatively constrain layer offset across the fault (Allmendinger, 1998). Although the restoration is arranged in steps back from the present for the sake of clarity, some of the steps undoubtedly overlap in time. For example, antithetic fault B is presumed to be active concurrently with the main fault.

In Figure 6b, we first remove the uplift of the Kingston Arch by restoring the Seattle Basin to its flexural shape. The 1.5–2 km of estimated uplift is in agreement with the estimated ~1.5 km of eroded Blakeley Formation (Tb in Fig. 6a) in the Mobil Kingston well (Rau and Johnson, 1999). We propose that the Arch is a fault-propagation fold over a south-dipping, blind thrust fault (km 62 of Fig. 2b). Using the geometry of the fold's forelimb (Fig. 7c) and the method of Suppe (1985, p. 351), we calculate the dip of the blind reverse fault to be 41°–49°. For lack of a better constraint, we estimate the shortening represented by the uplift of the Arch by equating the uplifted area with the shortened area of a 20-km-thick upper crust. The total north–south shortening using this assumption is 1.2 km.

We then undo the motion on the antithetic fault B in the Seattle fault zone (Fig. 6c). Antithetic fault B is included to bring the sedimentary rocks of the Blakeley and Blakely Harbor Formations, now exposed near Restoration Point, from a depth of ~4 km to the surface and place them over basement in the hanging wall. We next revert the fault sys-

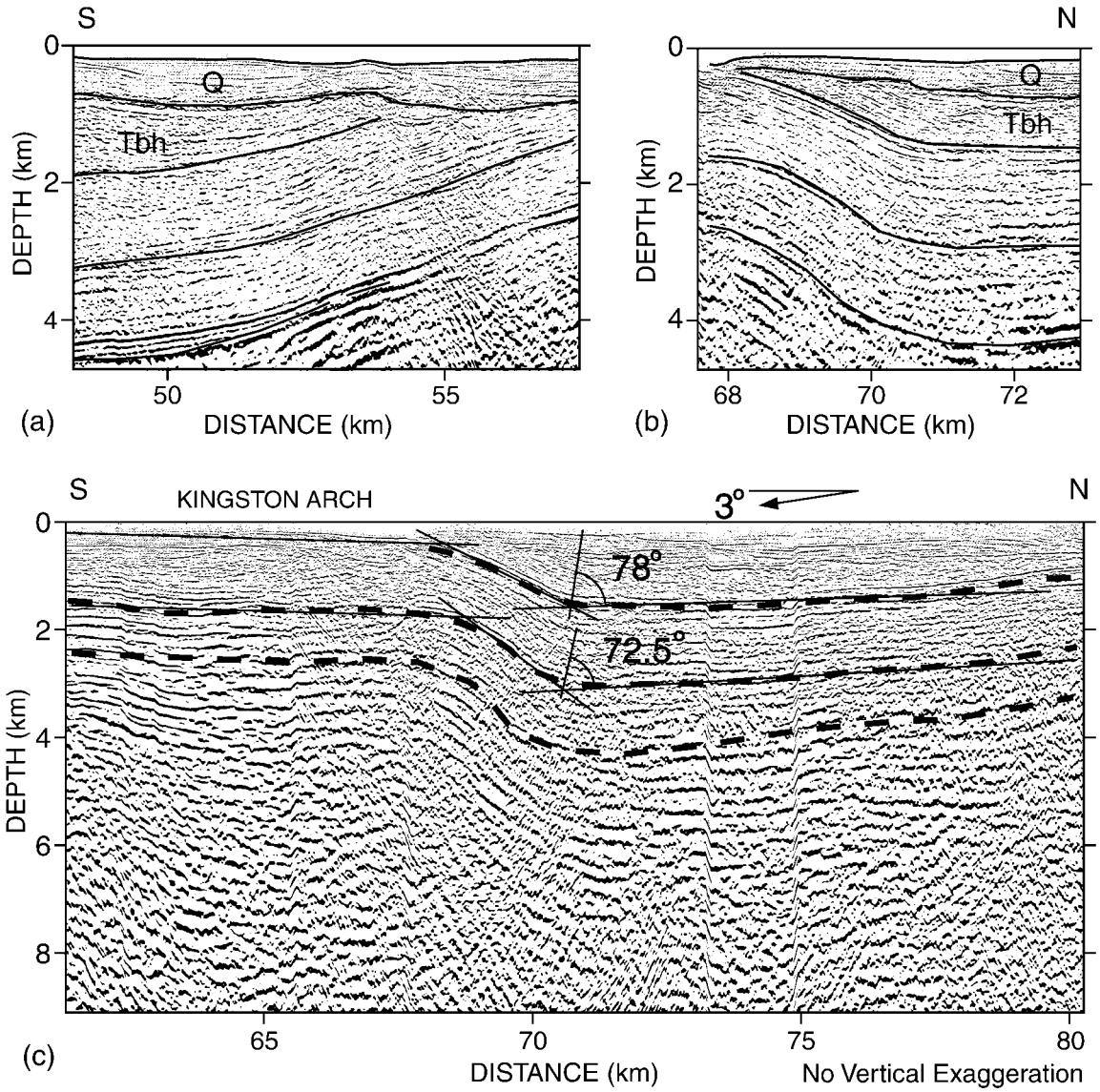

Figure 7. (a and b) Interpreted seismic-reflection profile on the flanks of Kingston Arch, showing strata tilted away from the Arch and possible offset in the Quaternary sediments, suggesting recent uplift of the Arch. See text for further details. (c) Enlargement of the seismic-reflection profile over Kingston Arch, showing synclinal angles used to estimate the dip of the buried reverse fault following the method of Suppe (1985). Location of sections is marked by frames in Figure 2a.

tem to a fault-propagation fold in the sediments. The fold may be manifested in the steeply dipping sediments above fault B that are observed in outcrops. Steeply dipping reflectors are not observed within the Crescent Formation below fault B (Fig. 2c), perhaps because the fold domain is expected to narrow considerably along the fault (e.g., Allmendinger, 1998) and be contained within the zone of chaotic reflections around fault A. The synclinal axis of the fold (thin, black line) should be steeper than the final fault trace (dashed red line) to enable the transfer of footwall sedimentary rocks, that is, Blakeley Formation in Restoration Point, to the hanging wall (Fig. 6d). Following Allmendinger (1998), we propose that the fold axial plane was ~8° steeper than the subsequent fault, because internal reflections within the Crescent Formation in the hanging wall (km 20–32 in Fig. 2b) appear to dip northward at this angle, and it is fair to assume that the hanging wall was originally horizontal. Erosion of the hanging wall well into the Crescent Formation is postulated in Figure 6c because the upper 60% of the Blakely Harbor Formation contain numerous, large clasts of Crescent Formation (Fulmer, 1975), implying that the Crescent Formation was exposed and eroded as the basin subsided. Crescent Formation rocks directly underlie glacial sediments south of the Seattle fault zone, according to in-

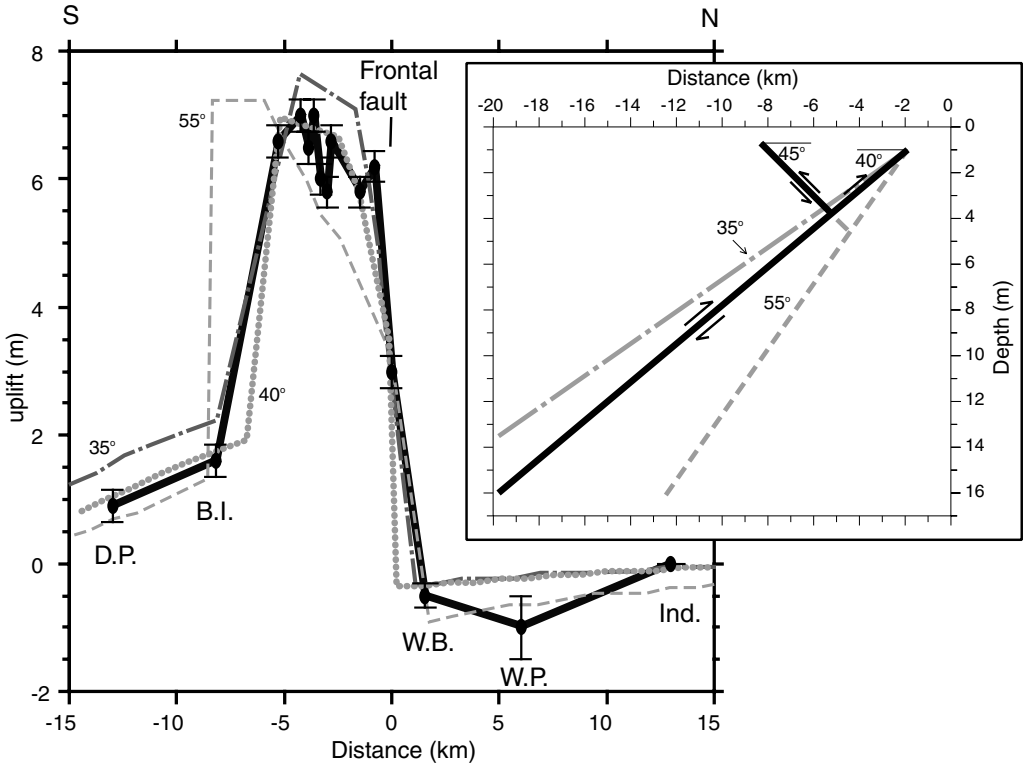

Figure 8. Shoreline uplift (heavy line) along Puget Sound projected along longitude 122°30′ W (after ten Brink and Bucknam, unpublished data) and calculated vertical displacement of the surface (gray lines) due to the fault configurations shown on the right. Origin corresponds to the location of the frontal fault trace of Blakely *et al.* (2001) at longitude 122°30′ W (see Fig. 1b for location). Vertical displacement was calculated using the program Coulomb 2.0 written by S. Toda, R. S. Stein, and G. C. P. King (Toda *et al.*, 1998). Abbreviated measurement locations are Ind., Indianola; W.P., West Point; W.B., Winslow Bay; B.I., Blake Island; D.P., Dolphin Point.

terpretations of seismic and gravity data (Figs. 2 and 5; Johnson *et al.*, 1994). The erosion of Crescent Formation rocks in the hanging wall is also consistent with the large throw on the Seattle fault, assuming that footwall subsidence and hanging-wall uplift are roughly of similar magnitude. In the final step, the fault-propagation fold is restored (Fig. 6e).

Before the development of the Seattle fault zone, the forearc region of Puget Lowland was covered by a several-kilometer-thick section of predominantly marine sediments, as evidenced in boreholes extending from north of Everett to south of Chehalis (Rau and Johnson, 1999). This sedimentary section is preserved under the Seattle Basin because of its later subsidence but is missing south of the fault zone because of its later uplift.

When Did the Seattle Fault Zone Start Its Activity?

Answering this question is necessary to estimate an average slip rate for the fault. We propose that reverse motion on the Seattle fault zone started when the region experienced uplift after the end of Blakeley Formation deposition at water depths >200 m (24.5 m.a.; Rau and Johnson, 1999) and before the start of Blakely Harbor Formation nonmarine deposition (shortly before 13.3 ± 1.3 m.a; B. Sherrod and J. Vance, personal comm., 2000). Blakeley Formation and older Eocene rocks maintain a relatively constant thickness within the Seattle Basin (Fig. 2). In contrast, the wedge of the Blakely Harbor sediments thickens toward the Seattle fault zone (Fig. 2) and was presumably deposited in a foreland basin created by the thrusting (Johnson *et al.*, 1994; Pratt *et al.*, 1997).

Earlier profiles of the Seattle Basin were interpreted to show a slight thickening of the Blakeley Formation sequence (Johnson *et al.*, 1994; Pratt *et al.*, 1997), although the criterion by which the Blakeley–to–Blakely Harbor sequence boundary in those profiles was defined was not specified. The boundary between the Blakeley and Blakely Harbor Formations is not encountered in nearby drill holes and cannot be extrapolated from outcrops. We define the boundary as an unconformity over which the lower part of the Blakely Harbor Formation sequence onlaps, because of the ~10 m.y. of hiatus between the deposition of the two formations (Rau and Johnson, 1999).

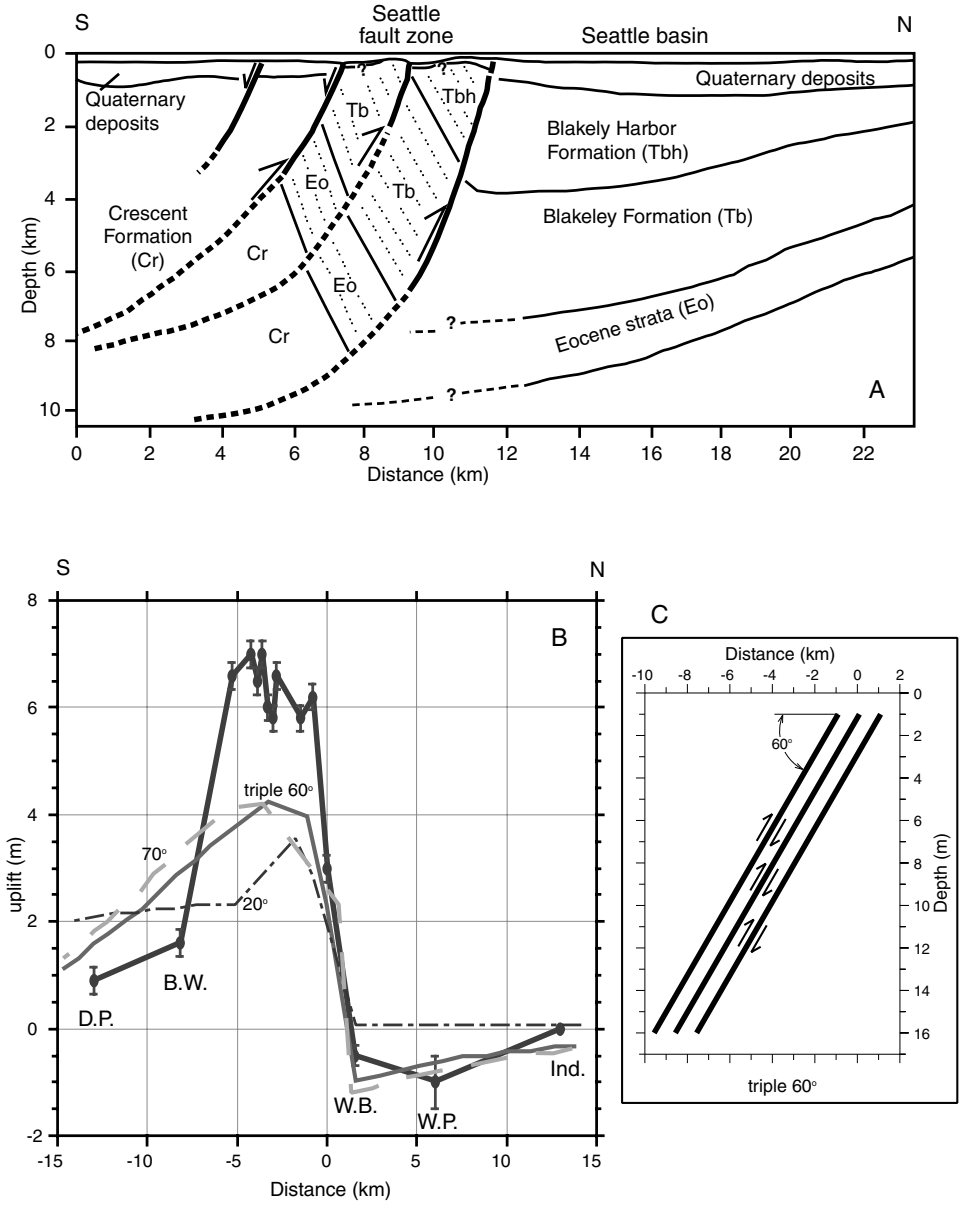

Figure 9. (A) Johnson's *et al.* (1994) configuration of the Seattle fault zone as a series of synthetic reverse faults with trapped sediments between them. (B) Shoreline uplift (heavy line) along Puget Sound projected along longitude 122°30′ W (after ten Brink and Bucknam, unpublished data) and calculated vertical displacement of the surface (thin lines) due to several fault configurations. Lines marked by 20° and 70° were calculated using geometry of a single reverse fault with that dip. Line marked triple 60° was calculated using fault geometry in C, which mimics Calvert and Fisher's (2001) suggested geometry of the Seattle fault zone based on shallow seismic-reflection data. Vertical displacement was calculated using Coulomb 2.0 program (Toda *et al.*, 1998). See text for discussion.

Johnson *et al.* (1994) suggested that reverse motion on the Seattle fault zone started in the late Eocene (~40 m.a.) because Crescent Formation conglomerate is exposed at the base of the Blakeley Formation in Restoration Point. However, this conglomerate is often rounded (Fulmer, 1975), and similar conglomerate can also be found in the preceding Eocene layer throughout the Puget Sound and as far as the northwestern corner of the Olympic Peninsula (Shilhanek, 1992; Rau and Johnson, 1999). Large variations in depositional environment and an unconformity are observed during this period in the region (Rau and Johnson, 1999). Therefore, Crescent Formation clasts did not have to come from the hanging wall of the Seattle fault. In addition, Blakeley Formation rocks throughout their thickness were regionally de-

posited at bathyal depths, which suggests regional subsidence, not uplift.

A middle Miocene age for the initiation of the Seattle fault zone matches the dates of a change in plate motion and the beginning of regional uplift and compressional deformation. Exhumation of the Olympic Peninsula started ~18 m.a., and stratigraphic and faunal indicators in the surrounding area indicate that uplift started in the middle Miocene (Brandon *et al.*, 1998). Major uplift of the forearc region in Oregon and Washington during the late middle Miocene (<15 m.a.) is indicated by a regional unconformity on the continental shelf and by folded rocks of the Miocene Astoria Formation and the Columbia River Basalts (Snavely *et al.*, 1996). On a larger scale, the Juan de Fuca Plate started rotating clockwise at 18 m.a. and seafloor spreading slowed. The clockwise rotation and the reduction in spreading rate aligned the Juan de Fuca Plate motion with respect to the Pacific Plate closer to that of the North American Plate, indicating that the Juan de Fuca Plate no longer moved independently.

A total slip of 10 km is estimated from the offset of Crescent Formation between the footwall of the Seattle fault zone and the surface, if we ignore the complications presented by antithetic fault B (Fig. 2b). This is a minimum estimate, because an unknown amount of Crescent Formation rocks were eroded from the hanging wall. If reverse motion on the Seattle fault zone started 15 m.y. ago, the average Neogene slip rate is 0.66 mm/yr. If ~2 km of Crescent Formation rocks were eroded from the hanging wall (Fig. 6c), the average Neogene slip rate is 0.87 mm/yr. A slip rate of 0.72–1.28 mm/yr for the Holocene can be deduced from the 8–14 m of uplift of glacial sediments (dated as post-17 k.y.) (Thorson, 1996), assuming that the uplift took place on a 40° fault. However, it is difficult to relate the long-term average slip to the Holocene slip rate because no other event similar in magnitude to the earthquake ~1,100 years ago has taken place in the past 7,500 years on the Seattle fault zone (Sherrod *et al.*, 1999).

Implications to Deformation Models of Puget Sound

Two models for the deformation of Puget Sound into a series of highs and basins have been proposed: a thin-skinned deformation along a detachment surface (Pratt *et al.*, 1997) and a thick-skinned deformation along steeply dipping reverse faults with opposing dips (Brocher *et al.*, 2001). If our interpretation of Seattle Basin stratigraphy as the result of both Seattle fault-zone loading and of a fault-propagating fold under the Kingston Arch is correct, then a deep detachment with a ramp (Pratt *et al.*, 1997) is not required. As explained in the Introduction, the ramp model was partly invoked to explain the shape of the Seattle Basin and Kingston Arch. We propose instead that the Seattle fault zone and the Kingston Arch are two south-dipping reverse faults and that the Seattle Basin is a disrupted flexural basin.

Brocher *et al.* (2001) proposed that the Seattle Basin is a sunken block between two high-angle reverse faults with opposing dips and that the Seattle Uplift and Kingston Arch are uplifted wedges between two high-angle reverse faults with opposing dips. The stratigraphy of the Seattle Basin along Puget Sound is inconsistent with sunken-block geometry, because the sediments do not dip both to the south and to the north. Instead, the sequences rise continuously from the Seattle Basin and onto the Kingston Arch (Fig. 2), and the arch itself is asymmetric with its steep flank facing north (Fig. 7).

Considering that the thickness of the Siletz terrane is 25–30 km, that is, deeper than the proposed detachment of Pratt *et al.* (1997), it is plausible that north–south shortening of the lowland is accomplished by thick-skinned reverse or thrust faults (Wells and Weaver, 1993; Brocher *et al.*, 2001) instead of thin-skinned ramps and faults. Brocher *et al.* (2001) proposed the existence of a north-dipping reverse fault south of the Seattle fault, the Tacoma fault. If the Tacoma fault exists, it should intersect the Seattle fault at depth, unless both faults are steeply dipping (>63° or >55° to avoid intersection at depths of 28 km and 20 km, respectively). Provided that the two faults are not steeply dipping and the Tacoma fault exists, either the Tacoma or the Seattle fault must act as a backthrust to the other fault.

Conclusions

The combination of independent data sets and different techniques for analysis and modeling provides additional information on the subsurface geometry of the Seattle fault zone and the Seattle Basin than was previously available. The Seattle Basin along Puget Sound reaches a maximum depth of 7 km; thins northward to the Kingston Arch, where it is <2.5 km thick; and thickens again north of the Kingston Arch. Dislocation models of Holocene shoreline uplift and subsidence along the western shore of Puget Sound underscore the need for an antithetic reverse fault at shallow depths to have ruptured together with the main trace of the Seattle fault to match the uplift and subsidence, which were presumably caused by an earthquake in the Seattle fault zone about ~900–930 A.D. The dislocation model, the P-wave-velocity field, and the modeled rock densities are inconsistent with the previously suggested geometry of the Seattle fault zone as a set of three or four parallel reverse faults (Johnson *et al.*, 1994, 1999; Calvert and Fisher, 2001). The dip of the Seattle fault remains elusive. Using the seismic-reflection and refraction data, we suggest that the fault has a dip range of 35°–45° down to a depth of 7 km, but we cannot put error bounds on this range. Using the dislocation model, the dip that fits the observed shoreline uplift is 35°–50°.

The Neogene sedimentary rocks in the Seattle Basin in the footwall of the Seattle fault zone are interpreted to have been deposited in a flexural basin formed by the load of the hanging wall. We interpret lithostratigraphic data from bore-

holes and the observed stratal geometry in the reflection data to indicate that reverse motion of the Seattle fault zone started some time between 24 and 14 m.a., and suggest that it was probably coincident with the initiation of regional uplift and compression in the forearc in the middle Miocene. According to our interpretation, this fault was initiated much later than the previously suggested late Eocene (~40 m.a.) date. Basin subsidence during the Neogene helped preserve the pre-Neogene sedimentary cover.

Disruption in the stratal geometry of the basin indicates Quaternary uplift of the Kingston Arch, located 30 km north of the Seattle fault zone. Microseismic activity there suggests ongoing uplift of the Arch. We interpret this uplift to be a fault-propagation fold over a reverse fault, with an estimated dip of 41°–49°. This interpretation contrasts with a previous interpretation of the Seattle Basin and Kingston Arch as shallow manifestations of a ramp in a midcrustal detachment (Pratt *et al.*, 1997). It is more likely that north–south shortening is accommodated by a series of thick-skinned reverse faults cutting perhaps the entire 25–30-km-thick Siletz terrane (Wells and Weaver, 1993; Brocher *et al.*, 2001). However, the observed basin stratigraphy is also inconsistent with the interpretation of the Seattle Basin as a sunken wedge between two high-angle reverse faults with opposing dips (Brocher *et al.*, 2001).

Acknowledgments

We thank Neal Driscoll, Sam Johnson, Ray Wells, Brian Atwater, Brian Sherrod, and Ross Stein for helpful discussions and T. Brocher, N. Driscoll, S. Johnson, R. Thorson, M. Brandon, T. Pratt, and C. Potter for their reviews. Support by the USGS coastal and marine geology and earthquake hazards programs is gratefully acknowledged.

References

Allmendinger, R. W. (1998). Inverse and forward numerical modeling of trishear fault-propagation folds, *Tectonics*, **17,** 640–656.

Atwater, B. F., and A. L. Moore (1992). A tsunami about 1000 years ago in Puget Sound, Washington, *Science* **258,** 1614–1617.

Blakely, R. J., R. E. Wells, C. S. Weaver, and S. Y. Johnson (2002). Location, structure, and seismicity of the Seattle Fault, Washington: evidence from aeromagnetic anomalies, geological maps, and seismic reflection data, *Geol. Soc. Am. Bull.* **114,** 169–177.

Brandon, M. T., M. K. Roden-Tice, and J. I. Garver, 1998, Late Cenozoic exhumation of the Cascadia accretionary wedge in the Olympic Mountains, northwest Washington State, *Geol. Soc. Am. Bull.* **10,** 985–11,009.

Brocher, T. M., and A. L. Reubel (1998). Compilation of 29 sonic and density logs from 23 oil test wells in western Washington State, *U.S. Geol. Surv. Open-File Rept.* **98–249,** 63 pp.

Brocher, T. M., T. Parsons, R. J. Blakely, N. I. Christensen, M. A. Fisher, R. E. Wells, and S. W. Group (2001). Upper crustal structure in Puget Lowland, Washington: results from the 1998 Seismic Hazards Investigation in Puget Sound, *J. Geophys. Res.* **106,** 13,541–13,564.

Bucknam, R. C., E. Hemphill-Haley, and E. B. Leopold (1992). Abrupt uplift within the past 1700 years at southern Puget Sound, Washington, *Science* **258,** 1611–1614.

Bucknam, R. C., B. L. Sherrod, G. Elfendahl, and S. D. Malone (1999). A fault scarp of probable Holocene age in the Seattle fault zone, Bainbridge Island, Washington *Seism. Res. Lett.* **70,** 233.

Calvert, A. J., M. A. Fisher, and the SHIPS working group (2001). Imaging the Seattle Fault zone with high-resolution seismic tomography, *Geophys. Res. Lett.* **28,** 2337–2340.

Crosson, R. S., N. P. Symons, and S. D. Malone (1999). A model for localization of seismicity in the central Puget Lowland, Washington, *Seism. Res. Lett.* **70,** 255.

Crosson, R. S., and N. P. Symons (2001). What goes down, comes up: flexural origin of the Puget basins and tectonic implications; *Seism. Res. Lett.* **72,** 237.

Duncan, R. A. (1982). A captured island chain in the coast range of Oregon and Washington, *J. Geophys. Res.* **87,** 10,827–10,837.

Erslev, E. A. (1991). Trishear fault-propagation folding, *Geology* **19,** 617–620.

Finn, C. A. (1990). Geophysical constraints on Washington convergent margin structure, *J. Geophys. Res.* **95,** 19,533–19,546.

Frankel, A. D., and W. Stephenson (2000). Three-dimensional simulations of ground motion in the Seattle region for earthquakes in the Seattle fault zone, *Bull. Seism. Soc. Am.* **90,** 1251–1267.

Fulmer, C. V. (1975). Stratigraphy and paleontology of the type Blakeley and Blakely Harbor formations, in *Conference on Future Energy Horizons of the Pacific Coast, Paleogene Symposium and Selected Technical Papers: 50th Annual Meeting of the Pacific Sections of AAPG, SEPM, and SEG*, D. W. Weaver, G. R. Hornaday, and A. Tipton (Editors), Long Beach, CA, pp. 210–271.

Gardner, G. H. F., L. W. Gardner, and A. R. Gregory (1974). Formation velocity and density; the diagnostic basics for stratigraphic traps, *Geophysics* **39,** 770–780.

Gower, H. D., J. C. Yount, and R. S. Crosson (1985). Seismotectonic map of the Puget Sound region, Washington, pp. 15 (1 sheet), U.S. Geological Survey Miscellaneous Investigations Series I-1613, scale 1:250,000.

Gueguen, Y., and V. Palciauskas (1994). Introduction to the Physics of Rocks, Priceton Univ Press, Princeton, NJ, 294 pp.

Johnson, S. Y., S. V. Dadisman, J. R. Childs, and W. D. Stanley (1999). Active tectonics of the Seattle Fault and central Puget Sound, Washington: implications for earthquake hazards, *Geol. Soc. Am. Bull.* **111,** 1042–1053.

Johnson, S. Y., C. J. Potter, and J. M. Armentrout (1994). Origin and evolution of the Seattle fault and Seattle Basin, Washington, *Geology* **22,** 71–74.

Johnson, S. Y., C. J. Potter, J. M. Armentrout, J. J. Miller, C. A. Finn, and C. S. Weaver (1996). The southern Whidbey Island fault: an active structure in the Puget Lowland, Washington, *Geol. Soc. Am. Bull.* **108,** 334–354.

Khazaradze, G., A. Qamar, and H. Dragert (1999). Tectonic deformation in western Washington from continuous GPS measurements, *Geophys. Res. Lett.* **26,** 3153–3156.

King, G. C., R. S. Stein, and J. B. Rundle (1988). The growth of geological structures by repeated earthquakes, 1; conceptual framework, *J. Geophys. Res.* **93,** 13,307–13,318.

Loss, J., I. A. Pecher, and U. S. ten Brink (1998). RayGUI: a graphical user interface for interactive ray-tracing (rayinvr), *U.S. Geol. Surv. Open-File Rept.* **98–203**.

Parsons, T., R. E. Wells, M. A. Fisher, E. Flueh, and U. S. ten Brink (1999). Three-dimensional velocity structure of Siletzia and other accreted terranes in the Cascadia forearc of Washington, *J Geophys. Res.*, **104,** 18,015–18,039.

Pezzopane, S. K., and R. J. Weldon II (1993). Tectonic role of active faulting in central Oregon, *Tectonics* **12,** 1140–1169.

Pratt, T. L., S. Y. Johnson, C. J. Potter, W. J. Stephenson, and C. A. Finn (1997). Seismic reflection images beneath Puget Sound, western Washington State: the Puget Lowland thrust sheet hypothesis, *J. Geophys. Res.*, **102,** 27,469–27,489.

Rau, W. W., and S. Y. Johnson (1999). Well stratigraphy and correlations, western Washington and northwest Oregon, *U.S. Geol Surv Map Invest. I-2621*, (3 sheets).

Sherrod, B. L., Bucknam, R. C., and Leopold, E. B. (1999). Holocene

relative sea level changes along the Seattle Fault at Restoration Point. *Q. Res.* **54,** 384–393.

Shilhanek, A. B. (1992). The sedimentology, petrology and tectonic significance of the middle Eocene Flattery Breccia, Lyre Formation, northwestern Olympic Peninsula, Washington, *M.A. Thesis*, Western Washington University, 150 pp.

Snavely, P. D. Jr., and R. E. Wells (1996). Cenozoic evolution of the continental margin of Oregon and Washington, in *Assessing Earthquake Hazards and Reducing Risk in the Pacific Northwest, Vol. 1*, in *U.S. Geol. Surv. Profes. Pap.*, pp. 161–182.

Suppe, J. (1985) Principles of Structural Geology, Prentice-Hall, Englewoods Cliffs, NJ, 537 pp.

Symons, N. P., and R. S. Crosson (1997). Seismic velocity structure of the Puget Sound region from three-dimensional nonlinear tomography, *Geophys. Res. Lett.* **24,** 2593–2596.

Thorson, R. M. (1996). Earthquake recurrence and glacial loading in western Washington, *Geol. Soc. Am. Bull.* **108,** 1182–1191.

Toda, S., R. S. Stein, P. A. Reasenberg, J. H. Dieterich, and A. Yoshida (1998). Stress transferred by the 1995 $M_w = 6.9$ Kobe, Japan, shock: effect on aftershocks and future earthquake probabilities, *J. Geophys. Res.* **103,** 24,543–24,565.

Trehu, A. M., I. Asudeh, T. M. Brocher, J. H. Luetgert, W. D. Mooney, J. L. Nabelek, and Y. Nakamura (1994). Crustal architecture of the Cascadia Forearc, *Science* **266,** 237–243.

van Wagoner, T. M., R. S. Crosson, K. C. Creager, G. Medema, L. Preston, N. P. Symons, and T. M. Brocher (2002). Crustal structure and relocated earthquakes in the Puget Lowland, Washington from high-resolution seismic tomography, *J. Geophys. Res.* (in press).

Walcott, R. I. (1993). Neogene tectonics and kinematics of western North America, *Tectonics* **12,** 326–333.

Wells, R. E., and C. S. Weaver (1993). Block deformation in Puget Lowland, in *Proceedings of the National Earthquake Prediction Evaluation Council*, V. E. Frizzel (Editor), *U.S. Geol. Surv. Open-File Rep.* **93–333,** 14–16.

Wells, R. E., C. S. Weaver, and R. J. Blakely (1998). Fore-arc migration in Cascadia and its neotectonic significance, *Geology* **26,** 759–762.

Yount, J. C., and H. D. Gower (1991). Bedrock geologic map of the Seattle 30′ by 60′ Quadrangle, Washington, *U.S. Geol. Surv. Open-File Rept. 91–147*, 37 pp. (4 sheets)

Zelt, C. A., and R. B. Smith (1992). Seismic traveltime inversion for 2D crustal velocity structure, *Geophys. J. Interiors* **108,** 16–34.

Zhang, J., and M. N. Toksoz (1998). Nonlinear refraction traveltime tomography, *Geophysics* **63,** 1726–1737.

Zoback, M. L., R. C. Jachens, and J. A. Olson (1999). Abrupt along-strike change in tectonic style: San Andreas fault zone, San Francisco Peninsula, *J. Geophys. Res.* **104,** 10,719–10,742.

U.S. Geological Survey
384 Woods Hole Rd.
Woods Hole, Massachusetts 02543
(U.S.t.B., P.C.M.)

U.S. Geological Survey
345 Middlefield Rd., MS 977
Menlo Park, California 94025
(M.A.F., R.J.B., T.P.)

U.S. Geological Survey
P.O. Box 25046
Lakewood, Colorado 80225
(R.C.B.)

Geophysics
Box 351650
University of Washington
Seattle, Washington 98195
(R.S.C., K.C.C.)

Manuscript received 23 August 2001.